

## Article

# Structure-Catalytic Properties Relationship in Friedel Crafts Alkylation Reaction for MCM-36-Type Zeolites Obtained by Isopropanol-Assisted Pillaring

Karolina Ogorzały<sup>1</sup>, Agnieszka Węgrzyn<sup>1</sup> , Aleksandra Korzeniowska<sup>1</sup>, Andrzej Sławek<sup>1,2</sup> ,  
Andrzej Kowalczyk<sup>1</sup> , Barbara Gil<sup>1,\*</sup> , Wiesław J. Roth<sup>1</sup> and Waclaw Makowski<sup>1,\*</sup> 

<sup>1</sup> Faculty of Chemistry, Jagiellonian University, Gronostajowa 2, 30-387 Kraków, Poland; karolina.ogorzaly@doctoral.uj.edu.pl (K.O.); a.m.wegrzyn@uj.edu.pl (A.W.); aleksandra.korzeniowska@uj.edu.pl (A.K.); aslawek1990@gmail.com (A.S.); andrzej.kowalczyk@uj.edu.pl (A.K.); wieslaw.roth@uj.edu.pl (W.J.R.)

<sup>2</sup> Academic Centre for Materials and Nanotechnology, AGH University of Science and Technology, al. Mickiewicza 30, 30-059 Kraków, Poland

\* Correspondence: barbara.k.gil@uj.edu.pl (B.G.); wacław.makowski@uj.edu.pl (W.M.); Tel.: +48-12-686-2469 (B.G.); +48-12-686-2471 (W.M.)

**Abstract:** MWW type zeolites are characterized by the presence of zeolitic layers of 2.5 nm thickness, containing 10-member ring sinusoidal channels inside and supercavities with 12-member ring openings located on their surfaces. Expansion and pillaring of layered zeolites increase the access to active sites and can enable or facilitate catalytic activity towards larger reactant molecules. This goal is explored in this work reporting the pillaring of layered zeolite MCM-56 with MWW topology by tetraethylorthosilicate (TEOS) treatment with the assistance of isopropanol, aimed at obtaining hierarchical micro-mesoporous systems. MCM-56 (Si/Al = 12) was synthesized with hexamethyleneimine as a structure-directing and aniline as a structure-promoting agent. Hierarchical porous systems were obtained using two different pillaring methods: (1) with TEOS only and (2) with TEOS mixed with isopropanol. The MWW framework was preserved during swelling/pillaring in both methods. Pillared zeolites obtained via alcohol-assisted pillaring possessed unique intermediate micro-mesopores with the size of about 2 nm. IR study revealed a decrease in the concentration of accessible acid centers upon pillaring. However, the fraction of acid sites on the external surface, accessible for adsorption of large molecules, increased by up to 90%. Catalytic activity was evaluated in the Friedel-Crafts alkylation of mesitylene with benzyl alcohol. Pillaring resulted in reduction of the acid site concentrations, but the materials retained high catalytic activity. Pillaring in the presence of alcohol produced increased turnover frequency values based on the concentrations of the external acid sites.

**Keywords:** layered zeolites; MCM-36; MCM-56; alcohol-assisted pillaring; catalysis; Friedel-Crafts alkylation



**Citation:** Ogorzały, K.; Węgrzyn, A.; Korzeniowska, A.; Sławek, A.; Kowalczyk, A.; Gil, B.; Roth, W.J.; Makowski, W. Structure-Catalytic Properties Relationship in Friedel Crafts Alkylation Reaction for MCM-36-Type Zeolites Obtained by Isopropanol-Assisted Pillaring. *Catalysts* **2021**, *11*, 299. <https://doi.org/10.3390/catal11030299>

Academic Editor: Benoît Louis

Received: 29 January 2021

Accepted: 22 February 2021

Published: 25 February 2021

**Publisher's Note:** MDPI stays neutral with regard to jurisdictional claims in published maps and institutional affiliations.



**Copyright:** © 2021 by the authors. Licensee MDPI, Basel, Switzerland. This article is an open access article distributed under the terms and conditions of the Creative Commons Attribution (CC BY) license (<https://creativecommons.org/licenses/by/4.0/>).

## 1. Introduction

The layered material MCM-56 is a unique representative of two-dimensional (2D) zeolites as a delaminated form obtained by direct synthesis with high activity and ease of modification [1–5]. It is the first layered zeolite exfoliated directly by soft-chemical treatment. MCM-56 can show activity higher than the conventional MWW forms MCM-22 and MCM-49 [6] but is an intermediate during the preparation of MCM-49 and, upon prolonged synthesis, it converts to this 3D form. Recently, Xing et al. [7] reported that addition of aniline to the MCM-56 synthesis delays the conversion to MCM-49 so it can be viewed as the final product (referred to as ‘temperature-controlled phase transformation’). Aniline is called a structure-promoting agent which facilitates crystallization but is not trapped within the framework; thus, it efficiently prevents layer condensation. Jiang

et al. [8] proposed an easy double templating method to control the crystallization of MCM-56, involving addition of tetraethyl ammonium hydroxide (TEAOH) to the HMI-containing synthesis mixture. This synthetic route yielded pure, delaminated MCM-56 material, with an extended phase stabilization period. The original MCM-56 prepared with HMI only has been extensively studied with regard to swelling and pillaring [4]. To the best of our knowledge, there seems to be no reports concerning modification of the MCM-56 obtained with the additives mentioned above [9].

The structure of MCM-56 is described as two-dimensional (2.5 nm thick MWW layers stacked randomly with only accidental interlayer bonds) [1]. Acid centers located on the surface of the layers may potentially catalyze reactions of bulky molecules [10]. As a common modification, a two-step process is often applied to open the structure and enhance accessibility of the acid centers by creating additional porosity between the zeolite layers through expansion of the interlayer space by swelling or intercalation followed by stabilization (e.g., pillaring with tetraethylorthosilicate/TEOS) or complete layer separation (delamination). The original pillared MWW zeolite was called MCM-36 [11]. Ultrasound treatment has been reported to facilitate exfoliation and layer dispersion [3,12–14] but if layers are coated with surfactant (hydrophobic surface), the separation would entail exposure to hydrophilic environment. This should favor the status quo rather than enhanced separation. Of course, there may be mechanical enhancement due to fracturing of the layers.

Increased accessibility of acid centers in expanded layered zeolites makes them attractive as catalysts for the transformation of large organic molecules. The Friedel-Crafts reaction is most often carried out in the liquid phase with the use of halogens as alkylation agents and acid homogeneous catalysts, e.g.,  $\text{FeCl}_3$ ,  $\text{AlCl}_3$ ,  $\text{BF}_3$ . Their application is associated with problems related to corrosion of the installation as well as recovery, separation, regeneration and disposal of the toxic catalyst waste [15]. Due to stricter environmental protection requirements, attempts are being made to replace homogeneous catalysts with solid acids (e.g., zeolites) [16] and perform alkylation reactions using alkyl alcohols instead of chlorides. MWW zeolites have shown particular benefits in this regard.

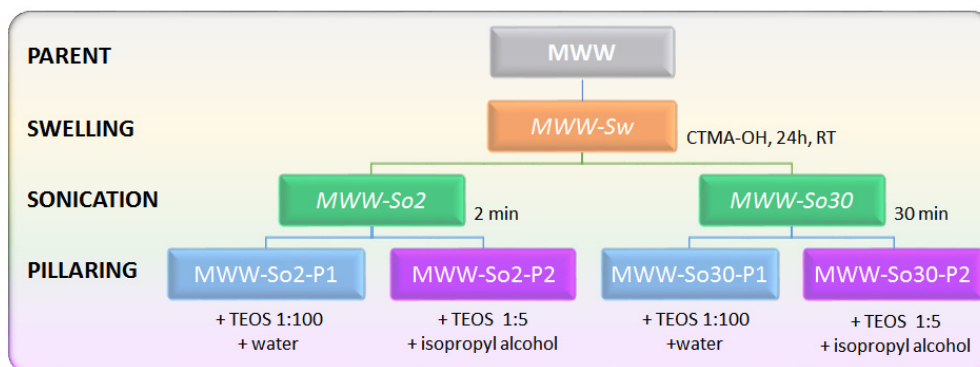
The aim of this work was to explore two pillaring procedures involving sonication treatment in an attempt to increase availability of the active centers. One procedure was adopted from the standard swelling and pillaring method often employed for modification of MWW zeolites, using excess amount of TEOS [3,11]. The other pillaring method was based on work by Letaïef et al. [17], in which alcohols were used as a medium controlling hydrolysis of TEOS in pillaring of layered clays. These authors concluded that their system allows better controlled TEOS hydrolysis and may be an attractive alternative not only for clays but also other layered solids. Herein, this method is applied to MCM-56 as a model layered zeolite material. The obtained modified zeolites were tested in Friedel-Crafts alkylation of mesitylene with benzyl alcohol, a reaction involving bulky organic molecules, designed to test the activity of the external surfaces of the zeolites [10,18].

## 2. Results and Discussion

The general outline of post-synthetic modifications of MCM-56 zeolite employed in this study is presented in Scheme 1. P1 denotes classical pillaring with the excess amount of TEOS, while P2, pillaring with TEOS in the presence of isopropanol. All of the final products were calcined in air at 540 °C. Detailed description of the synthesis and modifications is presented in Section 3.1.

The analysis of the XRD patterns has shown that the basic MCM-56 (MWW) structure of all studied materials has been preserved during applied modifications. This identification is based on the position of the intralayer 100 reflection ( $2\theta = 7.2^\circ$ , Cu  $K\alpha$  radiation used throughout) and the presence of a wide “band” without the dip between  $2\theta = 8\text{--}10^\circ$  indicating the lack of layer ordering in the c direction (Figure 1b). The fact that position of the intralayer reflection (100) remains unchanged upon modification confirms that the internal structure of the MWW layers is preserved. The emergence of maxima at lower  $2\theta$

angles (Figure 1a) indicates maintained layer separation after pillaring. The 001 reflection is observed with expanded materials and interlayer d-spacings ranges from 4.34 to 4.65 nm depending on the material (Table 1).



**Scheme 1.** Modification of the parent MWW (MCM-56) zeolite leading to the formation of swelled, sonicated (intermediate materials indicated in italics) and pillared MWW materials: MWW-So2-P1, MWW-So2-P2, MWW-So30-P1, MWW-So30-P2.

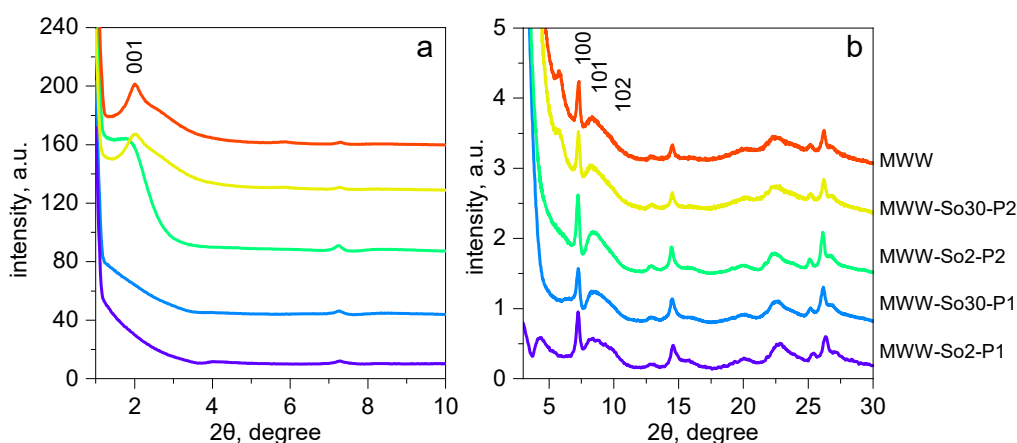


**Figure 1.** X-ray powder diffraction (XRD) patterns of the studied MWW zeolites in the range (a)  $2\theta = 1\text{--}10^\circ$ , (b)  $2\theta = 3\text{--}30^\circ$ .

**Table 1.** Structural and textural parameters of the MWW zeolites under study.

Sample	XRD 001	N <sub>2</sub> Sorption				QE-TPDA
		BET, m <sup>2</sup> /g	S <sub>ext</sub> , m <sup>2</sup> /g	V <sub>meso</sub> , cm <sup>3</sup> /g	V <sub>micro</sub> , cm <sup>3</sup> /g	V <sub>micro</sub> <sup>*</sup> cm <sup>3</sup> /g
MWW	-	469	183	0.04	0.10	0.08
MWW-So2-P1	-	580	197	0.16	0.05	0.12
MWW-So30-P1	4.65	872	245	0.28	0.06	0.13
MWW-So2-P2	4.34	733	148	0.22	0.04	0.18
MWW-So30-P2	4.34	779	143	0.25	0.03	0.16

\* calculated from the QE-TPDA profiles of hexane.

The nitrogen adsorption-desorption isotherms are shown in Figure 2a. The isotherm exhibited by the parent material (MCM-56, denoted as MWW) is characteristic for a microporous solids with significant external surface area, reaching almost 40% of the total surface area (469 and 183 m<sup>2</sup>/g, respectively) and some large, most probably interparticle mesopores, as suggested by a wide, H2b-type hysteresis loop [19]. Isotherms for all modified samples show considerable increase of adsorption, corresponding to secondary mesoporosity introduced upon swelling and pillaring. The materials synthesized with the use of isopropanol (the P2 series: MWW-So2-P2 and MWW-So30-P2) exhibit increased

adsorption at low relative pressure ( $p/p^0$  up to 0.3), isotherms without hysteresis loops, revealing presence of wide micropores or narrow mesopores. It is evident that in the case of two other pillared samples (the P1 series: MWW-So2-P1 and MWW-So30-P1), adsorption isotherms are of type IV with H4 hysteresis loops. Closing of the hysteresis loop at  $p/p^0$  equal to 0.5 is usually attributed to the presence of ink-bottle mesopores or interconnected, partially constricted mesopore systems. In this case, this would correspond to the overlapping effects of formation of narrow intraparticle mesopores, formed due to pillaring and much wider and less ordered interparticle mesopores.

The findings based on the  $N_2$  adsorption data were corroborated by the results of Quasi-Equilibrated Temperature Programmed Desorption and Adsorption (QE-TPDA) of hexane and nonane. This characterization method, developed for characterization of micro- and mesoporous materials, has been proven useful in studies of modified zeolites [20–25]. The QE-TPDA profiles are recorded while the studied sample is cyclically heated and cooled in the flow of helium containing small admixture (<1 mol%) of the hydrocarbon vapor. The maxima that were recorded during heating correspond to desorption from the pores, while the minima that were observed during cooling correspond to adsorption. The higher the adsorption/desorption temperature, the smaller the corresponding pore size. By judicious choice of the adsorbate, its content in the carried gas and the heating/cooling rate, one may select a range of the pore sizes for detailed analysis.

The QE-TPDA profiles of hexane (Figure 2b) are restricted to the adsorption in the micropores, since they were recorded at low relative partial pressure of the adsorptive, far from the saturation conditions (200 mbar at 25 °C). They exhibit narrow maxima at about 50 °C, observed just after starting heating of the sample in the desorption phase of the QE-TPDA experiment. These maxima represent larger micropores (e.g., distorted structural ones) or the strongest adsorption sites either on the external surface or on the surface of the mesopores. They are most intense for the –P2 (pillared with isopropanol present) zeolites, for which high contribution of wide micropores or narrow mesopores was found. Additional wide maxima that are observed in the high temperature range (100–200 °C) correspond to structural micropores formed by 10-rings channels, characteristic for the MWW layers. It is evident that to some extent that these micropores were retained after pillaring (Table 1). However, as it is not possible to separate the low and high temperature desorption peaks in the QE-TPDA profiles of hexane, especially for the modified zeolites. In this technique, one may expect the presence of a broad continuous distribution of the pore sizes in the micropore region. For this reason, the micropore volumes calculated by integration of these profiles are larger than those obtained from the  $N_2$  adsorption data, especially for the pillared materials.

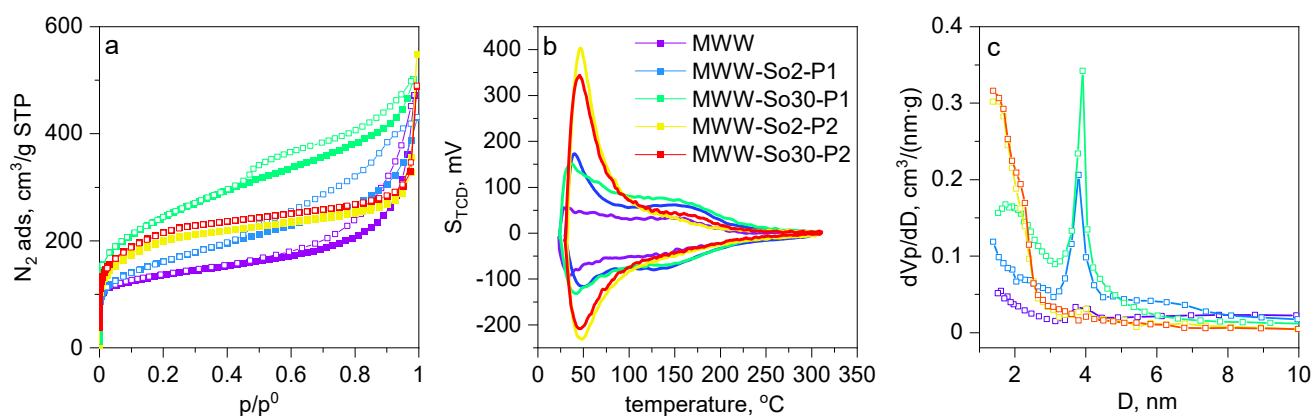


**Figure 2.** (a)  $N_2$  adsorption-desorption isotherms at  $-196\text{ °C}$ , (b) Quasi-Equilibrated Temperature Programmed Desorption and Adsorption (QE-TPDA) profiles of n-hexane, (c) pore size distribution for MWW zeolites under study.

The differences in porosity of the studied materials are better illustrated in Figure 2c showing pore size distributions, calculated from the desorption branches of the  $N_2$  sorption

data, using the BJH scheme. For the -P2 materials modified with the use of isopropanol, the calculations confirm the presence of unique intermediate pores with the size of about 2 nm, while the P1 materials also contain larger mesopores with broad pore size distributions (4–10 nm in the case of MWW-So2-P1). As noted on previous occasions [26], sharp peaks at 4 nm are common in modified layered materials and do not correspond to actual pore sizes, but result from the instability of liquid-like adsorbate at relative pressures below  $0.45 p/p^0$ . For more detailed porosity analysis, the NLDFT method was applied. The corresponding plots are shown in Figure S1.

Generally, the type of porosity shown by the modified materials for the classically pillared samples (the P1 series) seem to depend also on the sonication time: the longer the sonication, the higher the mesopore volume and the external surface area (Table 1, 0.16 vs. 0.28  $\text{cm}^3/\text{g}$  and 197 vs. 245  $\text{m}^2/\text{g}$ , for the samples sonicated for 2 and 30 min, respectively). Interestingly, the micropore volume remains almost unchanged (the small increase from 0.05 to 0.06  $\text{cm}^3/\text{g}$  is within the measurement accuracy). This would corroborate the conclusion that apart from the formation of intralayer mesopores, the mutual layer arrangement changed, hence the presence of the interlayer mesopores of wide size distribution. The porosity of the -P2 series is practically independent of the sonication time—for samples sonicated for 2 and 30 min, both the mesopore volumes and external surface area are similar (0.22 vs. 0.25  $\text{cm}^3/\text{g}$ , and 148 vs. 143  $\text{m}^2/\text{g}$ ). These would correspond to the mechanism, proposed by Letaïef [17], where hydrolysis of TEOS in presence of alcohol resulted in the pillared structure in which mainly the interlayer ordering was influenced.

The acid sites in aluminosilicates may be either of Brønsted or Lewis character. Acidic protons may come from Si-OH-Al groups (strong Brønsted acid sites)—the primary source of strong acid activity, surface silanols (non-acidic or weak Brønsted acid sites), or acidic OH groups associated with extraframework or partially framework Al species (usually weak Brønsted acid sites). Figure 3 shows that for the studied materials the external, terminal silanols are characterized by the IR band at  $3747 \text{ cm}^{-1}$  and the intensity of this band systematically increased and widened upon modification (better seen in Figure S2). This is consistent with the introduction of amorphous silica as the pillaring material. Additionally, for pillared samples the main position of this band moves to  $3743 \text{ cm}^{-1}$ , which is characteristic of internal silanols located at the structural defects, including geminal silanols  $\text{Si}(\text{OH})_2$ , due to the presence of OH groups from pillars made of amorphous  $\text{SiO}_2$ . Hydroxyls associated with extraframework or partial framework Al ( $3670 \text{ cm}^{-1}$ ) is visible in the spectrum of the parent material and the sample MWW-So2-P1. For all others, this band is practically invisible, and even if present, it may be hidden under the wide silanol tail that is characteristic of amorphous silica.

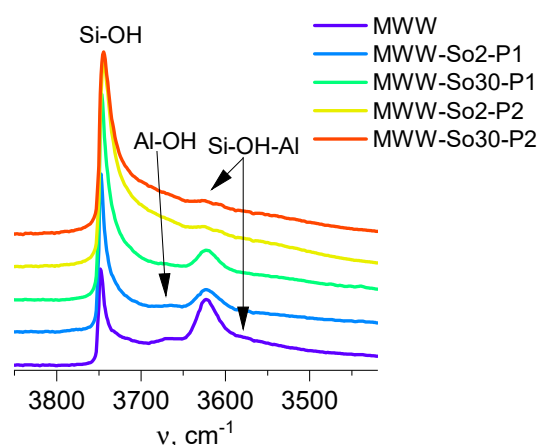


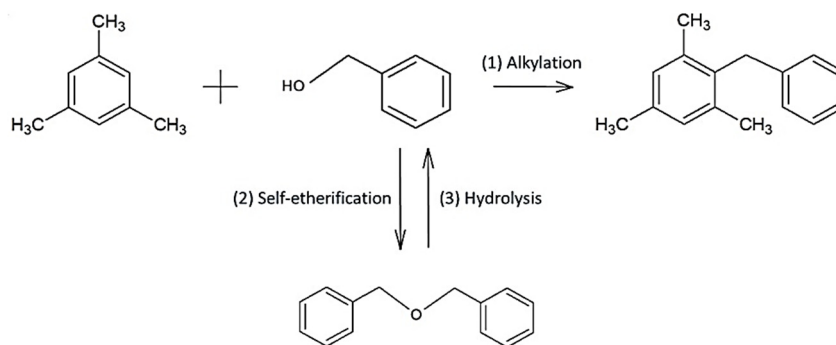
**Figure 3.** IR spectra in the OH region for MWW zeolites under study. All samples activated at  $470 \text{ }^\circ\text{C}$ , all spectra at RT, normalized to a 10 mg pellet.

The Si-OH-Al hydroxyls, the strong Brønsted acid sites (BAS) for MWW structure are characterized by IR bands at  $3624\text{ cm}^{-1}$  with a very weak shoulder at ca.  $3575\text{ cm}^{-1}$  (marked by two arrows in Figure 3). The former maximum corresponds to OH located in supercages, external cups and 10-member rings, while the latter to the OH groups in the double six-membered rings connecting the supercages (corresponding to the OH group connected with the unusual, hidden T3 position of the Al atom) [27,28].

The intensity of the  $3624\text{ cm}^{-1}$  maximum gradually decreases upon modification, which corresponds to a BAS concentration decrease from 900 to  $140\text{ }\mu\text{mol/g}$ . It can be deduced that sonication time (2 vs. 30 min) has less effect on the acidity than pillaring procedure. The samples from the -P1 series were pillared with TEOS only, at the 1:100  $w/w$  ratio, and therefore with substantial excess of silica. In contrast, the -P2 samples showed only small TEOS excess (1:5  $w/w$  ratio) in the presence of the isopropyl alcohol. It is interesting to note that the concentration of acid centers in samples pillared with higher TEOS concentration is in fact much higher than for samples pillared with much lower TEOS concentration. At the same time, the amount of Al, determined by XRF, is not considerably decreased. The simplest explanation for this is that deposited silica covers the Al sites and blocks access to them. Other factors cannot be ruled out, e.g., migration of Al atoms into other (non-Brønsted) locations.

Judging solely on the concentration of the BAS in the final pillared samples, the alcohol-aided procedure proposed by the group of Ruiz-Hitzky [17] would appear not to be optimal for layered zeolites, since its value is reduced by 70–80% compared to the classic pillaring (Table 2, Figure S4, BAS concentration 514 vs. 171, and 671 vs.  $136\text{ }\mu\text{mol/g}$ , comparing MWW-So2-P1 with MWW-So2-P2 and MWW-So30-P1 with MWW-So30-P2, respectively) and decreases by more than 90% in comparison to the parent material (initial BAS concentration  $899\text{ }\mu\text{mol/g}$ ). This had only a minor effect on the overall conversion but at the same time enhanced turnover frequency, indicating there may be benefits to the isopropanol assisted pillaring.

The goal of pillaring is an enhancement of mesoporosity to increase activity towards larger molecules. To evaluate this result, the Friedel-Crafts alkylation of mesitylene with benzyl alcohol was carried as the model test reactions. The main product in this reaction is 2-benzyl-1,3,5-trimethylbenzene (BTB), with dibenzyl ether (DBE) being the only side product (Scheme 2).



**Scheme 2.** Representation of the test reaction, the Friedel-Crafts alkylation of the mesitylene with benzyl alcohol.

To investigate the catalytic properties/activity of the studied MWW materials, we performed catalytic experiments in the liquid phase batch reactor. Figure 4a shows characteristic kinetic curves with linear dependence of conversion vs. time, implying constant reaction rate (or zero order kinetics). The 100% conversion of benzyl alcohol was obtained after ca. 180 min. Initially, formation of dibenzyl ether was observed (with maximum selectivity of ca. 10%), but later it was completely transformed to the main product (benzylated mesitylene) (Figure 4b).

Comparison of the kinetic curves (Figure 4a) shows high activity of the parent zeolite, with  $t_{1/2}$  equal 56 min (Table 2). Kinetic curves observed for all of the modified materials exhibited smaller slopes (i.e., lower overall reaction rate). However, comparison of the turnover frequency (TOF) data shows considerable increase of individual activity of the acid centers, especially in the materials pillared according to the P2 method (alcohol addition). Low values of acid sites concentration found for the P2 series may indicate high content of the amorphous silica introduced during modification, despite smaller TEOS excess. This seems justified by long reaction time of the pillared zeolite with TEOS.

The rate of the secondary reaction (transformation of DBE to BTB) was the slowest for the -P2 series, followed by the P1 one, while the transformation of DBE to BTB was the fastest for the parent material, but this is due to different overall reaction rate. If conversion vs. selectivity is drawn, then at the same conversion level there is no difference in selectivities (Figure S3).

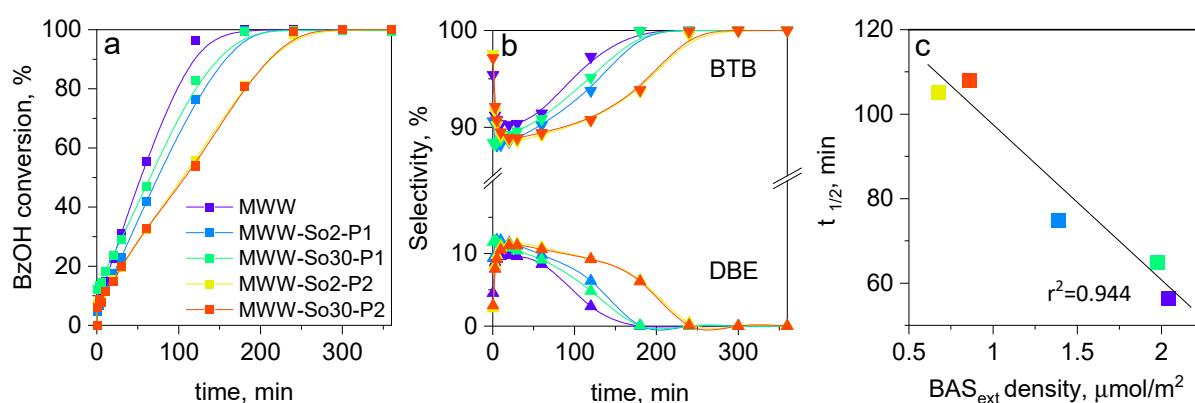


**Figure 4.** (a) Benzyl alcohol conversion in Friedel-Crafts alkylation of the mesitylene with benzyl alcohol, (b) selectivity to benzyl-1,3,5-trimethylbenzene (BTB) and dibenzyl ether (DBE) and (c) dependence of the reactivity values (in term of  $t_{1/2}$ ) on the density of the Brønsted acid sites located at the external layer surfaces ( $BAS_{ext}$ ).

**Table 2.** Acid and catalytic properties of MWW zeolites under study.

Sample	Si/Al		Acid Site Concentration, $\mu\text{mol}/\text{g}$				$BAS_{ext}$		TOF, $10^{-3} \text{ s}^{-1}$		$t_{1/2}$ , min
	XRF	BAS + LAS	BAS <sup>a</sup>	BAS <sup>b</sup>	LAS	BAS <sub>ext</sub>	Share, %	Density	BAS <sup>c</sup>	BAS <sub>ext</sub> <sup>d</sup>	
MWW	12	12	18	899	108	374	42	2.042	1.69	5.18	56
MWW-So2-P1	10	13	31	514	169	273	53	1.388	2.09	3.96	75
MWW-So30-P1	11	10	24	671	234	484	72	1.975	1.69	2.28	65
MWW-So2-P2	17	42	96	171	57	100	59	0.676	4.41	5.43	105
MWW-So30-P2	19	55	122	136	42	123	90	0.859	5.23	5.83	108

BAS<sup>a</sup>—Si/Al value relative to Brønsted acid sites only; BAS<sup>b</sup>—concentration of Brønsted acid sites; BAS<sup>c</sup>—turnover frequency (TOF) relative to Brønsted acid sites only; BAS<sub>ext</sub><sup>d</sup>—turnover frequency (TOF) relative to Brønsted acid sites only.

Lower concentration of the BAS in modified samples explains lower reaction rates and longer reaction half-time. On the other hand, it is important to note that even if BAS concentration dropped almost 7-fold (from 899 to 135  $\mu\text{mol}/\text{g}$ ), the 100% conversion is reached after 120 min for parent material and after ca. 240 min for MWW-So30-P2. It is evident that a single acid center becomes more active, which can be expressed quantitatively by calculation of the TOF values. The TOF values are the highest for materials pillared in the presence of alcohol ( $4.41 \times 10^{-3}$  and  $5.23 \times 10^{-3} \text{ s}^{-1}$  for MWW-So2-P2 and MWW-So30-P2, respectively) comparing to  $1.69 \times 10^{-3}$  and  $2.09 \times 10^{-3} \text{ s}^{-1}$  for other samples. This may also be linked to the availability of the acid centers to bulky molecules. To check this availability, additional IR measurements were carried out and involved the adsorption of pivalonitrile (PN), a molecule which cannot diffuse through 10-membered rings in MWW zeolite and therefore can be used to quantify the BAS on the external surfaces

( $BAS_{ext}$ , Table 2). It is evident that, even if the overall concentration of BAS decreased upon modifications, the accessibility increased (from 42% in the parent MWW, to 90% in MWW-So30-P2). Unfortunately, the decrease in BAS concentration was not compensated by the increased availability of these centers, and the actual concentration of  $BAS_{ext}$  increased only for MWW-So30-P1 (from 374 to 474  $\mu\text{mol/g}$ ) but decreased for any other sample. It should be noted that MWW-So30-P1, even though it possessed the highest concentration of the external acid sites, was not the most active. It seems that the important factor is  $BAS_{ext}$  density, corresponding to their actual accessibility for the reactants, calculated as the  $BAS_{ext}$  concentration divided by the external surface ( $S_{ext}$ ). If reactivity (in term of  $t_{1/2}$ ) was plotted against  $BAS_{ext}$  density, the dependence was linear (Figure 4c).

Another important factor influencing the catalytic activity of an individual acid center may be their acid strength. Acid strength may be determined either by the adsorption of strong bases, leading to proton transfer, or by the interaction with weaker bases, leading to the formation of a hydrogen bond. Both processes may be followed by IR spectroscopy. Acid strength, determined by thermodesorption of bases, may depend not only on the intrinsic strength of acid sites, but also on the presence or absence of diffusion limitations. In other words, diffusion may be slowed down in micropores falsely implying higher acid strength to OH groups located there. Adsorption of weaker bases, like CO, more directly depends on the intrinsic acid strength—the higher the red-shift of the IR maximum of given OH group upon interaction with the weak base, the stronger the acid center [29]. This method has also drawbacks, since a hydrogen-bonded molecule may also interact with surrounding oxygens defining the zeolitic channel, and is subjected to channel size-dependent dispersive interactions [30]. However, it has been proposed that the CO molecule are less influenced than other molecules ( $N_2$  or acetonitrile) [31].

In the present investigation, both methods were applied for three selected samples: MWW, MWW-So30-P1, and MWW-So30-P2. CO was adsorbed, the value of the red-shift of the Si-OH-Al groups was determined and compared with the results of pyridine thermodesorption (Figure 5 and Figure S5, Table S1). The value of the bathochromic shift was comparable for all samples (312 to 325  $\text{cm}^{-1}$ ). In the study of pyridine thermodesorption, the fraction of the pyridinium ions still present after each desorption step was also comparable for all samples. Therefore, it may be concluded that the results of both experiments indicate no significant difference in the acid strength among the studied samples, and therefore the concentration of accessible BAS centers have the biggest influence on the catalytic activity.

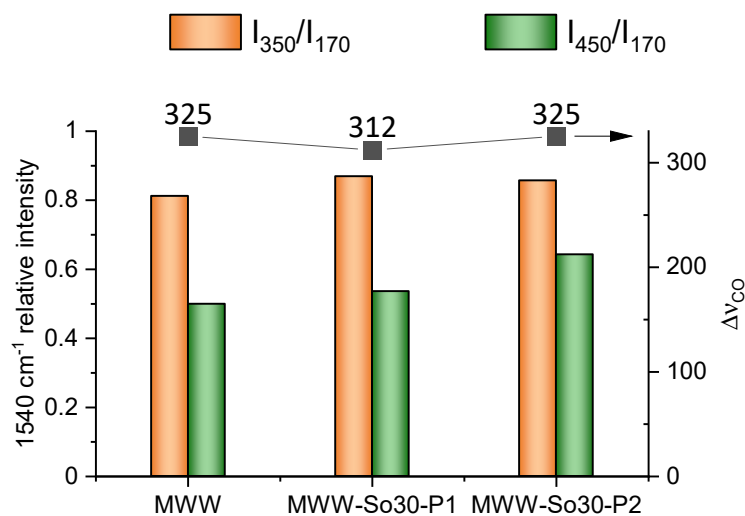


**Figure 5.** The values of OH groups red shift upon CO adsorption ( $\Delta\nu_{CO}$ ) and the intensities of pyridine  $1540\text{ cm}^{-1}$  band after thermodesorption at 350 and 450  $^{\circ}\text{C}$ , relative to the intensity after Py adsorption at 170  $^{\circ}\text{C}$  ( $I_{350}/I_{170}$  and  $I_{450}/I_{170}$ ).

### 3. Materials and Methods

#### 3.1. Catalyst Synthesis

MCM-56 zeolite with aniline (AN) was synthesized according to the procedure described in the literature [32]. The synthesis mixture comprised deionized water, 50% NaOH solution (Sigma Aldrich Poland, Poznań, Polska), sodium aluminate (Riedel-de-Haen, Seelze, Germany, 40–45% Na<sub>2</sub>O, 50–56% Al<sub>2</sub>O<sub>3</sub>), hexamethyleneimine (HMI, 99%, Sigma Aldrich Poland, Poznań, Polska), aniline (AN, > 99%, Sigma Aldrich Poland, Poznań, Polska) and Aerosil (A200, Evonic, Piscataway, NJ, USA) in the following molar ratios: Si/Al = 12.5, OH/Si = 0.18, HMI/Si = 0.1, AN/Si = 0.2 and H<sub>2</sub>O/Si = 45. The crystallization was carried out in a Teflon-lined autoclave (200 mL) at 143 °C for 352 h, static approximately half of the time and then rotated till completion. The products were isolated by centrifugation, washed three times with distilled water and dried in air. The parent MCM-56 sample is denoted as MWW.

Swelling process was carried out using cetyltrimethylammonium hydroxide solution (CTMA-OH, made in-house) [33]. The mixtures, containing 0.5 g of as-made MCM-56 and 20 g CTMA-OH, were stirred for 24 h at room temperature. The products were isolated by centrifugation, washed three times with distilled water and dried in air.

The swollen samples were sonicated using Ultrasonic Processor VCX 130 (Sonics & Materials, Newtown, CT, USA) with stepped microtips (70% amplitude), either for 2 min (denoted as MWW-So2) or 30 min. (denoted as MWW-So30), acidified with HCl to pH below 2, separated, washed with water (three times) and dried in air [3].

In the first series (–P1), pillaring of the swollen and sonicated zeolite was carried out using tetraethylorthosilicate (TEOS, Sigma Aldrich Poland, Poznań, Polska) with 1:100 *w/w* ratio [34]. The reaction mixtures were stirred at RT for 24 h. The solids were filtered on a Büchner funnel (without washing) and dried at room temperature in air.

In the second series (–P2), after swelling with CTMA-OH, the zeolites were pillared with an addition of isopropyl alcohol. The wet solids obtained after centrifugation from swelling agent were washed three times with distilled water. Immediately afterwards, 13 mL of 2-propanol was added, and the mixtures were stirred for 2 h. After that, 2.6 g tetraethylorthosilicate (TEOS) was added (1:5 *w/w* ratio in relation to the initial zeolite mass), and then the mixtures were stirred for 7 days at RT. The solids were filtered on a Büchner funnel (without washing) and dried at room temperature in air.

The final products were obtained after calcination at 540 °C for 6 h in air (ramp at 2 °C/min) and exchange with 1M NH<sub>4</sub>NO<sub>3</sub> solution (three times, 0.5 g of the zeolite in 20 mL of solution, 1 h at room temperature), washed with deionized water, dried, and activated at 500 °C.

#### 3.2. Catalyst Characterization

X-ray powder diffraction (XRD) was carried out using a Bruker AXS D8 Advance diffractometer (Bruker, Billerica, MA, USA) equipped with a graphite monochromator (Bruker, Billerica, MA, USA), position sensitive detector (Vântec-1, Bruker, Billerica, MA, USA) in Bragg-Brentano geometry in the range 1–10° 2 $\theta$  and Rigaku MiniFlex diffractometer (Rigaku, TheWoodlands, TX, USA) in reflection mode. CuK $\alpha$  radiation ( $\lambda$  = 0.154 nm) was used in the ranges 3–30° 2 $\theta$ . The XRD patterns were collected with steps of 0.02°.

Relative content of Al and Si was determined in the samples formulated into pellets, 13 mm in diameter, with the use of Energy-Dispersive XRF spectrometer (Thermo Scientific, ARL QUANT'X, Waltham, MA, USA). The X-rays of 4–50 kV (1 kV step) with the beam size of 1 mm were generated with the Rh anode. The detector used was a 3.5 mm Si(Li) drifted crystal with a Peltier cooling (ca. –90 °C). For quantitative analysis, calibration with a series of metallic standards and UniQuant software (Version 3, Thermo Fisher, West Palm Beach, FL, USA) were used.

Characterization of Lewis (LAS) and Brønsted (BAS) acid sites was carried out using adsorption of pyridine (absorption coefficients:  $\epsilon_{\text{LAS}} = 0.165 \text{ cm}^2/\mu\text{mol}$ , and  $\epsilon_{\text{BAS}} = 0.044 \text{ cm}^2/\mu\text{mol}$ ), pivalonitrile and CO [35,36] followed by IR spectroscopy (Tensor 27 from

Bruker, Billerica, Ettlingen, Germany, MTC detector, spectral resolution  $2\text{ cm}^{-1}$ ). Zeolites were pressed into self-supporting wafers and activated in situ at  $500\text{ }^\circ\text{C}$  for 1 h at high vacuum ( $10^{-5}$  mbar) in a home-made quartz cell, equipped with  $\text{CaF}_2$  windows. The cell construction allowed in situ activation, measurement of the spectra at chosen temperature and adsorption of gases and vapors inside the infrared spectrometer. Before adsorption of a probe molecule the system was cooled to the proper adsorption temperature:  $170\text{ }^\circ\text{C}$  for pyridine (Py), ambient temperature for pivalonitrile (PN), and ca.  $-100\text{ }^\circ\text{C}$  for CO. After adsorption of the vapors (ca. 20 mbar equilibrium pressure for Py and PN, and ca. 5 mbar for CO) the gas phase together with weakly adsorbed species were evacuated at the adsorption temperature for 20 min (Py and PN) and 1 min for CO. In pyridine thermodesorption experiments, additional desorption steps at  $350$  and  $450\text{ }^\circ\text{C}$  were performed (20 min each), after each desorption sample was cooled down to  $170\text{ }^\circ\text{C}$  and the spectrum collected. All spectra were recalculated to the same pellet mass, equal 10 mg.

Nitrogen isotherms were determined by the standard method at  $-196\text{ }^\circ\text{C}$  (liquid nitrogen temperature) using an ASAP2025 (Micromeritics, Norcross, GA, USA) static volumetric apparatus and autosorb iQ Gas Sorption System (Quantachrome, Boynton Beach, FL, USA). Before experiments, the samples were outgassed at  $350\text{ }^\circ\text{C}$  using a turbomolecular pump to remove pre-adsorbed water.

The porosity was also studied by quasi-equilibrated temperature programmed desorption and adsorption (QE-TPDA, home-made equipment) of hexane. The instrumentation and experimental procedures were described in detail previously [20–22]. Prior to the QE-TPDA measurements a sample (6–7 mg) placed in a quartz tube was activated by heating up to  $400\text{ }^\circ\text{C}$  ( $10\text{ }^\circ\text{C}/\text{min}$ ) in flow of helium ( $7\text{ cm}^3/\text{min}$ ), then cooled to room temperature. After activation, the hexane vapor was added to the helium stream resulting in isothermal sorption at room temperature. The signal of the thermal conductivity detector, consisting of desorption maxima and adsorption minima, recorded during cyclic heating and cooling of the sample at constant rate, represented a QE-TPDA profile.

The catalytic test reaction, liquid phase alkylation of mesitylene with benzyl alcohol, was carried out in a three-necked round-bottom equipped with a reflux condenser with heating in a multi-experiment workstation StarFish (Radleys Discovery Technologies, Saffron Walden, UK) under atmospheric pressure. The reaction temperature was  $80\text{ }^\circ\text{C}$ . First, reaction samples were activated at  $500\text{ }^\circ\text{C}$  for 5 h in air. Then 22 mL of mesitylene, 50 mg of the studied catalyst and 0.1 g of dodecane, as an internal standard, were mixed. The reaction mixture was maintained for 30 min at  $80\text{ }^\circ\text{C}$  and then 0.2 g of benzyl alcohol was added. This was considered as the beginning of the reaction. Liquid samples (0.4 mL) were withdrawn at regular intervals (0.5, 3, 5, 10, 20, 30, 60, 120, 180, 240, 300, and 360 min) and analyzed by the gas chromatograph PerkinElmer Clarus 600 GC (PerkinElmer, Shelton, CT, USA) with an FID detector (PerkinElmer, Shelton, CT, USA) using a 30 m packed column Elite-1MS (PerkinElmer, Shelton, CT, USA).

#### 4. Conclusions

MCM-56 synthesized with HMI as the primary template and aniline as the structure promoter was expanded with surfactants and pillared by two post-synthesis methods—the standard one using large excess of TEOS (100:1, TEOS:solid), denoted P1 series, and a novel one based on hydrolysis of TEOS in the presence of isopropanol, the P2 series, and evaluated as acid catalysts based on textural parameters, FTIR characteristics, and model catalytic reaction designed for probing activity towards bulky reactants.

The MWW framework was preserved during swelling/pillaring in both methods. Also, both modification procedures resulted in the formation of secondary mesoporosity and increase of the external surface area. The P2 zeolites obtained via alcohol-assisted pillaring possessed unique intermediate micro-mesopores with the size of about 2 nm. There was practically no influence of sonication time on porosity of the P2 modified zeolites. In the case of the P1 zeolites, after prolonged sonication the standard pillaring procedure yielded very high external surface and secondary mesopores showing broad distribution

of pore sizes. Zeolite MWW-So2-P1 after short sonication exhibited much smaller surface area and larger mesopore pore sizes.

IR study revealed a decrease in the concentration of accessible acid centers upon pillaring, which was much more pronounced for the P2 series. However, the fraction of acid sites on the external surface, accessible for adsorption of large molecules, increased considerably upon modifications, especially for the P2 zeolites (from 42% to 59% for the -P1 or 90%, for the -P2).

Despite decreased acidity, the modified zeolites retained high catalytic activity. The P2 zeolites demonstrated increased turnover frequency values calculated based on the concentrations of the external acid sites, which may be exploited to look for optimal pillaring extent/activity balance.

**Supplementary Materials:** The following are available online at <https://www.mdpi.com/2073-4344/11/3/299/s1>, Figure S1: Pore size distribution for MWW zeolites under study calculated using NLDFT method; Figure S2: IR spectra in the OH region for MWW zeolites under study. All spectra at RT, normalized to a 10 mg pellet. Alternative representation of Figure 4 in the main paper; Figure S3: Dependence of the BTB and DBE selectivity on the reaction time (a,b) and BzOH conversion (c,d), Figure S4: IR spectra of pyridine adsorbed on MWW zeolites under study. All spectra at 170 °C, normalized to a 10 mg sample. The IR maxima used to calculate the concentration of Brønsted acid sites (BAS) and Lewis acid sites (LAS) are marked as Py-BAS and Py-LAS; Figure S5: IR spectra of CO adsorbed on chosen MWW zeolites. All spectra at -100 °C, normalized to a 10 mg sample, (a) MWW; (b) MWW-So30-P1; (c) MWW-So30-P2; (d) difference spectra (activated sample minus after CO adsorption) for all three zeolites.; Table S1: The values of OH groups red shift upon CO adsorption ( $\Delta\nu_{\text{CO}}$ ) and the intensities of pyridine 1540  $\text{cm}^{-1}$  band after thermodesorption at 350 and 450 °C, relative to the intensity after Py adsorption at 170 °C ( $I_{350}/I_{170}$  and  $I_{450}/I_{170}$ ).

**Author Contributions:** K.O., W.M. and B.G.; methodology: K.O., B.G., A.W. and W.M.; experimental investigations: K.O., A.K. (Aleksandra Korzeniowska), A.S., A.K. (Andrzej Kowalczyk); data curation: K.O., A.K. (Aleksandra Korzeniowska), A.S., A.K. (Andrzej Kowalczyk); writing—original draft preparation: K.O., B.G. and W.M.; writing—review and editing: B.G., W.M. and W.J.R.; visualization: B.G. All authors have read and agreed to the published version of the manuscript.

**Funding:** This work was financed with the funds from the National Science Centre Poland, grant no 2016/21/B/ST5/00858. K.O. has been partially supported by the EU Project POWR.03.02.00-00-I004/16.

**Data Availability Statement:** Data is contained within the article or supplementary material.

**Conflicts of Interest:** The authors declare no conflict of interest.

## References

1. Roth, W.J. MCM-22 zeolite family and the delaminated zeolite MCM-56 obtained in one-step synthesis. In *Studies in Surface Science and Catalysis*; Elsevier: Amsterdam, The Netherlands, 2005; pp. 19–26.
2. Juttu, G.G.; Lobo, R.F. Characterization and catalytic properties of MCM-56 and MCM-22 zeolites. *Microporous Mesoporous Mater.* **2000**, *40*, 9–23. [[CrossRef](#)]
3. Gil, B.; Makowski, W.; Marszałek, B.; Roth, W.J.; Kubu, M.; Čejka, J.; Olejniczak, Z. High acidity unilamellar zeolite MCM-56 and its pillared and delaminated derivatives. *Dalt. Trans.* **2014**, *43*, 10501. [[CrossRef](#)]
4. Roth, W.J.; Čejka, J.; Millini, R.; Montanari, E.; Gil, B.; Kubu, M. Swelling and Interlayer Chemistry of Layered MWW Zeolites MCM-22 and MCM-56 with High Al Content. *Chem. Mater.* **2015**, *27*, 4620–4629. [[CrossRef](#)]
5. Xu, L.; Wu, P. Diversity of layered zeolites: From synthesis to structural modifications. *New J. Chem.* **2016**, *40*, 3968–3981. [[CrossRef](#)]
6. Cheng, J.C.; Fung, A.D.; Klocke, D.J.; Lawton, S.L.; Lissy, D.N.; Roth, W.J.; Smith, C.M.; Walsh, D.E. Process and zeolitic catalysts for preparing short chain alkyl aromatic compounds. *Zeolites* **1995**, *5*, 453–554.
7. Xing, E.; Shi, Y.; Xie, W.; Zhang, F.; Mu, X.; Shu, X. Perspectives on the multi-functions of aniline: Cases from the temperature-controlled phase transfer hydrothermal synthesis of MWW zeolites. *Microporous Mesoporous Mater.* **2017**, *254*, 201–210. [[CrossRef](#)]
8. Jiang, L.; Li, X.; Gong, Y.; Meng, X.; Zhang, L.; Zhai, Y.; Shang, S.; Meng, L. MCM-56 stabilization synthesis using auxiliary tetraethylammonium ions: Its role to inhibit surface Si-O-Al bridged linkage and retain highly delaminated structure. *Microporous Mesoporous Mater.* **2020**, *302*, 110245. [[CrossRef](#)]

9. Shamzhy, M.; Gil, B.; Opanasenko, M.; Roth, W.J.; Čejka, J. MWW and MFI Frameworks as Model Layered Zeolites: Structures, Transformations, Properties, and Activity. *ACS Catal.* **2021**, 2366–2396. [[CrossRef](#)]
10. Grzybek, J.; Roth, W.J.; Gil, B.; Korzeniowska, A.; Mazur, M.; Čejka, J.; Morris, R.E. A new layered MWW zeolite synthesized with the bifunctional surfactant template and the updated classification of layered zeolite forms obtained by direct synthesis. *J. Mater. Chem. A* **2019**, 7, 7701–7709. [[CrossRef](#)]
11. Roth, W.J.; Kresge, C.T.; Vartuli, J.C.; Leonowicz, M.E.; Fung, A.S.; McCullen, S.B. MCM-36: The first pillared molecular sieve with zeolite properties. In *Studies in Surface Science and Catalysis*; Elsevier: Amsterdam, The Netherlands, 1995; pp. 301–308.
12. Corma, A.; Fornes, V.; Pergher, S.B.; Maesen, T.L.M.; Buglass, J.G. Delaminated zeolite precursors as selective acidic catalysts. *Nature* **1998**, 396, 353–356. [[CrossRef](#)]
13. Maheshwari, S.; Jordan, E.; Kumar, S.; Bates, F.S.; Penn, R.L.; Shantz, D.F.; Tsapatsis, M. Layer structure preservation during swelling, pillaring, and exfoliation of a zeolite precursor. *J. Am. Chem. Soc.* **2008**, 130, 1507–1516. [[CrossRef](#)]
14. Thakkar, R.; Bandyopadhyay, R. Preparation, characterization, and post-synthetic modification of layered MCM-22 zeolite precursor. *J. Chem. Sci.* **2017**, 129, 1671–1676. [[CrossRef](#)]
15. Sartori, G.; Maggi, R. Use of Solid Catalysts in Friedel–Crafts Acylation Reactions. *Chem. Rev.* **2006**, 106, 1077–1104. [[CrossRef](#)] [[PubMed](#)]
16. Narender, N.; Mohan, K.V.V.K.; Kulkarni, S.J.; Reddy, I.A.K. Liquid phase benzoylation of benzene and toluene with benzyl alcohol over modified zeolites. *Catal. Commun.* **2006**, 7, 583–588. [[CrossRef](#)]
17. Letaïef, S.; Angeles Martín-Luengo, M.; Aranda, P.; Ruiz-Hitzky, E. A colloidal route for delamination of layered solids: Novel porous-clay nanocomposites. *Adv. Funct. Mater.* **2006**, 16, 401–409. [[CrossRef](#)]
18. Luo, H.Y.; Michaelis, V.K.; Hodges, S.; Griffin, R.G.; Román-Leshkov, Y. One-pot synthesis of MWW zeolite nanosheets using a rationally designed organic structure-directing agent. *Chem. Sci.* **2015**, 6, 6320–6324. [[CrossRef](#)] [[PubMed](#)]
19. Thommes, M.; Kaneko, K.; Neimark, A.V.; Olivier, J.P.; Rodriguez-Reinoso, F.; Rouquerol, J.; Sing, K.S.W. Physisorption of gases, with special reference to the evaluation of surface area and pore size distribution (IUPAC Technical Report). *Pure Appl. Chem.* **2015**, 87, 1051–1069. [[CrossRef](#)]
20. Makowski, W. Quasi-equilibrated temperature programmed desorption and adsorption: A new method for determination of the isosteric adsorption heat. *Thermochim. Acta* **2007**, 454, 26–32. [[CrossRef](#)]
21. Makowski, W.; Kuśtrowski, P. Probing pore structure of microporous and mesoporous molecular sieves by quasi-equilibrated temperature programmed desorption and adsorption of n-nonane. *Microporous Mesoporous Mater.* **2007**, 102, 283–289. [[CrossRef](#)]
22. Makowski, W.; Maňko, M.; Dudek, A.; Mlekodaj, K. Application of quasi-equilibrated thermodesorption of hexane and cyclohexane for characterization of porosity of zeolites and ordered mesoporous silicas. *Adsorption* **2013**, 19, 537–544. [[CrossRef](#)]
23. Roth, W.J.; Gil, B.; Makowski, W.; Sławek, A.; Grzybek, J.; Kubu, M.; Čejka, J. Interconversion of the CDO Layered Precursor ZSM-55 between FER and CDO Frameworks by Controlled Deswelling and Reassembly. *Chem. Mater.* **2016**, 28, 3616–3619. [[CrossRef](#)]
24. Roth, W.J.; Gil, B.; Makowski, W.; Sławek, A.; Korzeniowska, A.; Grzybek, J.; Siwek, M.; Michorczyk, P. Framework-substituted cerium MCM-22 zeolite and its interlayer expanded derivative MWW-IEZ. *Catal. Sci. Technol.* **2016**, 6, 2742–2753. [[CrossRef](#)]
25. Makowski, W.; Gil, B.; Majda, D. Characterization of Acidity and Porosity of Zeolite Catalysts by the Equilibrated Thermodesorption of n-Hexane and n-Nonane. *Catal. Lett.* **2008**, 120, 154–160. [[CrossRef](#)]
26. Thommes, M. Physical Adsorption Characterization of Nanoporous Materials. *Chem. Ing. Tech.* **2010**, 82, 1059–1073. [[CrossRef](#)]
27. Onida, B.; Geobaldo, F.; Testa, F.; Crea, F.; Garrone, E. FTIR investigation of the interaction at 77 K of diatomic molecular probes on MCM-22 zeolite. *Microporous Mesoporous Mater.* **1999**, 30, 119–127. [[CrossRef](#)]
28. Meloni, D.; Laforge, S.; Martin, D.; Guisnet, M.; Rombi, E.; Solinas, V. Acidic and catalytic properties of H-MCM-22 zeolites. *Appl. Catal. A Gen.* **2001**, 215, 55–66. [[CrossRef](#)]
29. Lavalley, J.C. Infrared spectrometric studies of the surface basicity of metal oxides and zeolites using adsorbed probe molecules. *Catal. Today* **1996**, 27, 377–401. [[CrossRef](#)]
30. Thang, H.V.; Vaculík, J.; Přeč, J.; Kubů, M.; Čejka, J.; Nachtigall, P.; Bulánek, R.; Grajciar, L. The Brønsted acidity of three- and two-dimensional zeolites. *Microporous Mesoporous Mater.* **2019**, 282, 121–132. [[CrossRef](#)]
31. Marie, O.; Massiani, P.; Thibault-Starzyk, F. Infrared Evidence of a Third Brønsted Site in Mordenites. *J. Phys. Chem. B* **2004**, 108, 5073–5081. [[CrossRef](#)]
32. Xing, E.; Shi, Y.; Xie, W.; Zhang, F.; Mu, X.; Shu, X. Temperature-controlled phase-transfer hydrothermal synthesis of MWW zeolites and their alkylation performances. *RSC Adv.* **2016**, 6, 29707–29717. [[CrossRef](#)]
33. Roth, W.J.; Chlubná, P.; Kubů, M.; Vitvarová, D. Swelling of MCM-56 and MCM-22P with a new medium—Surfactant–Tetramethylammonium hydroxide mixtures. *Catal. Today* **2013**, 204, 8–14. [[CrossRef](#)]
34. Roth, W.J.; Gil, B.; Mayoral, A.; Grzybek, J.; Korzeniowska, A.; Kubu, M.; Makowski, W.; Čejka, J.; Olejniczak, Z.; Mazur, M. Pillaring of layered zeolite precursors with ferrierite topology leading to unusual molecular sieves on the micro/mesoporous border. *Dalt. Trans.* **2018**, 47, 3029–3037. [[CrossRef](#)] [[PubMed](#)]
35. Gil, B.; Roth, W.J.; Makowski, W.; Marszałek, B.; Majda, D.; Olejniczak, Z.; Michorczyk, P. Facile evaluation of the crystallization and quality of the transient layered zeolite MCM-56 by infrared spectroscopy. *Catal. Today* **2015**, 243, 39–45. [[CrossRef](#)]
36. Gil, B.; Kałahurska, K.; Kowalczyk, A. A study of the external and internal sites of 2D and 3D zeolites through the FTIR investigation of the adsorption of ammonia and pivalonitrile. *Appl. Catal. A Gen.* **2019**, 578, 63–69. [[CrossRef](#)]